Ultrafast carrier dynamics, band-gap renormalization, and optical properties of ZnSe nanowires

Lin Tian (田琳),[1] Lorenzo di Mario,[1] Valentina Zannier,[2,*] Daniele Catone,[3] Stefano Colonna,[3] Patrick O'Keeffe,[4] Stefano Turchini,[3] Nicola Zema,[3] Silvia Rubini,[2] and Faustino Martelli[1,†]

[1]*Istituto per la Microelettronica e i Microsistemi-Consiglio Nazionale delle Ricerche, Via del fosso del cavaliere 100, 00133 Roma, Italy*
[2]*Istituto Officina dei Materiali-CNR, TASC Laboratory, Basovizza, 34149 Trieste, Italy*
[3]*Istituto di Struttura della Materia-CNR, Via del fosso del cavaliere 100, 00133 Roma, Italy*
[4]*Istituto di Struttura della Materia-CNR, Area della Ricerca di Roma 1, 00016 Monterotondo Scalo, Italy*

In this paper, we present a comprehensive study of the carrier dynamics and optical properties of ZnSe nanowires (NWs). The transparency of the sample, obtained by the growth of the ZnSe NWs on glass, allowed us to perform transmittance, reflectance, photoluminescence (PL), time-resolved PL, and pump-probe transient absorption spectroscopy on as-grown samples. All measurements were performed at room temperature. Strong light trapping at the band-gap energy has been observed in reflectivity measurements. Fast transient absorption bleaching due to band filling and band-gap renormalization has been observed. The band-gap renormalization has a rise time constant of about 170 fs and a decay time of about 4 ps. Fast transient absorption bleaching is also observed at energies below the band gap, suggesting that intrinsic processes prevail over extrinsic photoinduced transitions in our high-quality NWs. The PL reveals the presence at room temperature of excitonic emission that shows a decay time of 0.5 ns. All of these features indicate that our ZnSe NWs have quality comparable to epitaxial films and can be used for optical devices and nonlinear optics.

I. INTRODUCTION

Semiconductor nanowires (NWs) have attracted extensive interest in the last two decades because of their unique properties and numerous potential applications. One possible application of NWs is the fabrication of lasers [1,2]. ZnSe is a II-VI wide band-gap semiconductor suitable for light emission in the blue-green region of the visible spectrum. However, bulk or epitaxial ZnSe is considered to be inferior to its III-V competitor, GaN, as a reliable material for laser fabrication [3]. The reason lies in the point defects that are generated in the material under thermal stress, especially when it is grown on mismatched III-V substrates. On the other hand, ZnSe could become an interesting material within NW technology precisely because of the lack of lattice mismatch constrains offered by the NW geometry [4] and the possibility to grow it at low growth temperature (T_g), a condition that is known to be optimal for achieving good near band-edge (NBE) optical emission [5]. These features are technologically relevant because one interesting consequence is that NWs can be grown on any substrate that withstands the growth conditions. Therefore, ZnSe NWs can be grown on low-cost substrates, including glass (coated with transparent contact oxides for device fabrication) and plastics, materials that cannot withstand the high T_g needed to grow GaN NWs [6].

Despite the technological advantages of a low T_g and although the optimal growth temperature for ZnSe films with high optical quality is around 300 °C [5], ZnSe NWs are often grown at 520 °C and above [7–11]. The reason is the intent to favor the vapor–liquid–solid (VLS) growth mechanism [12], which involves liquid alloy nanoparticles

(NPs) during the growth. In the past, some of the present authors have demonstrated that solid Au particles can still promote the one-dimensional (1D) ZnSe growth and have developed the growth of ZnSe NWs by molecular beam epitaxy (MBE) at T_g as low as 300 °C [13–15]. The growths were performed on several substrates such as GaAs(111)B, Si(111), SiO$_2$, and indium-tin-oxide (ITO)–coated glass. We have shown that T_g strongly affects the optical properties and that only NWs grown at low T_g show a strong NBE luminescence, regardless of the nature of the substrate. In particular, very intense low-temperature (14 K) blue photoluminescence (PL) from ZnSe NWs grown at 300 °C on ITO-coated glass [14] was reported.

In order to use ZnSe NWs in optoelectronic devices, it is necessary to have a deep understanding of the carrier dynamics and optical properties in those nanostructures. Laser operation, indeed, strongly depends on emission efficiency, recombination lifetime, attainable carrier density, and carrier-phonon scattering.

In this paper, we present a thorough study of stationary and transient optical properties of ZnSe NWs grown at 300 °C by MBE. In particular, with the purpose of studying light emission and absorption on the same as-grown sample, we have investigated the ZnSe NWs grown on ITO-coated glass, which is transparent in the energy range of interest. We hence performed transmittance, reflectance, PL, time-resolved PL, and fast transient absorption spectroscopy on the same NW ensemble. All measurements were performed at room temperature. Dynamics of band-gap renormalization, excitonic contribution to the luminescence, and influence of defects are observed and discussed, offering a quite complete picture of the optical properties of ZnSe NWs.

II. EXPERIMENTAL DETAILS

The ZnSe NWs have been grown by MBE on ITO-coated glass at 300 °C. The samples consist of a very high density

---

*Present address: Istituto Nanoscienze - CNR and National Enterprise for nanoScience and nanoTechnology, Scuola Normale Superiore, Piazza S. Silvestro, 12, 56127 Pisa (Italy).

†faustino.martelli@cnr.it

of randomly oriented ZnSe NWs. They are tapered, with a mean diameter at the tip of 10 nm and base diameter 10 times larger, with an average length of about 1 μm. No shell protects the ZnSe NWs. Full details on the growth conditions, morphological and structural characterization as well as low-temperature luminescence can be found in Zannier *et al.* [14]. The PL and time-resolved PL have been performed using the second harmonic of a Ti:sapphire laser at 405 nm with a pulse length of 20 fs at 80 MHz repetition rate. The PL signal was analyzed using a 0.35 m long monochromator and a charge-coupled device (CCD) or a Si-APD [full width at half maximum (FWHM) = 150 ps] for quasistationary or time-resolved analysis, respectively. The fast transient absorption spectra were measured by pump-probe experiments. As a pump, we used the amplified second harmonic of a Ti:sapphire laser at 405 nm with a pulse length of about 50 fs at a 1 kHz repetition rate, and as a probe we used the continuum white light generated in a femtosecond transient absorption spectrometer of IB Photonics (FemtoFrame II). The pump-probe response was studied in the 350–750 nm wavelength range. We used pump fluences of 60 and 150 μJ/cm^2. No qualitative difference was found at the different excitation intensities except for long time delays, as explained in the Results section. Transmission and reflectivity measurements were performed in a Perkin-Elmer spectrophotometer equipped with an integration sphere.

III. RESULTS

Transmittance (T, black) and reflectance (R, red-dashed) curves are shown in Fig. 1(a). T (R) represents the ratio of the light intensity transmitted through (reflected from) the sample on the incident intensity. Both curves show a sharp decrease around 2.6 eV. From those curves, we can calculate the absorbance (A) using the equation [16],

$$A = \log_{10} \frac{(1-R)^2}{T}. \qquad (1)$$

According to Tauc and Menth's expression for thin films [17], we have $\alpha(h\upsilon) \cdot h\upsilon = B_0(h\upsilon - Eg)^m$, where $h\upsilon$ and Eg are the incident photon energy and the optical band gap, respectively, and $\alpha(h\upsilon)$ is the absorption coefficient and is related to absorbance by $\alpha(h\upsilon) = 2.303 \times A(h\upsilon)/d$, where d is the film thickness. Therefore, Tauc and Menth's expression can be rewritten as $(A(h\upsilon) \cdot h\upsilon)^{1/m} = B_1(h\upsilon - Eg)$, where $B_1 = (B_0 \cdot d/2.303)^{1/m}$ is a constant related to the film thickness and m is ½ for a direct band gap. In this way, the optical band gap can be extracted without knowing the film thickness, which is a very complex parameter for NW mats. The quantity $(A(h\upsilon) \cdot h\upsilon)^2$ is shown in Fig. 1(b). We deduce the optical band gap to be 2.63 eV, as extracted from the intercept between the linear extrapolation of $(A(h\upsilon) \cdot h\upsilon)^2$ and the energy axis. Along with the sharp increase of the absorbance at energies larger than the band gap, we observe a long Urbach's tail due to localized states.

Using fast transient absorption spectroscopy by means of a pump-probe experiment, we measure the variation of the sample absorbance after the excitation given by the pump pulse. To give an overview of the results, the complete
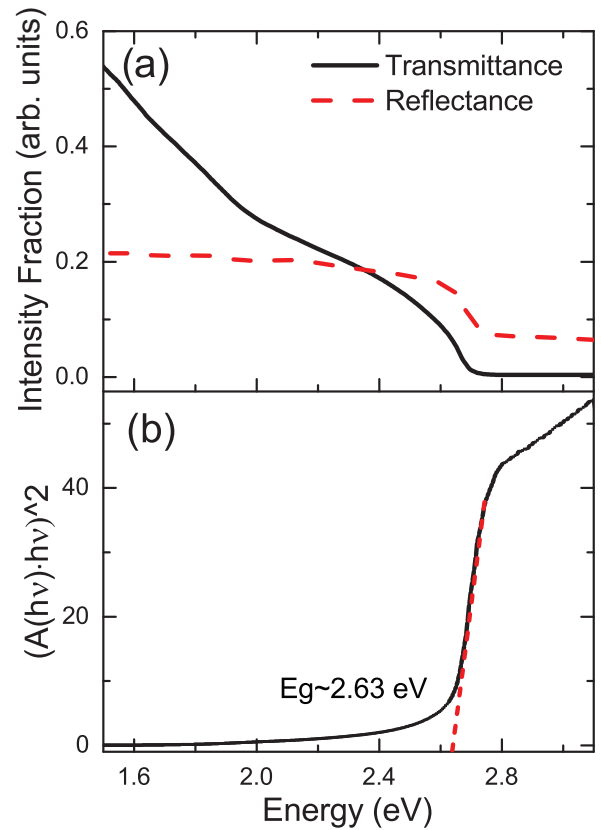
FIG. 1. (a) Transmittance (black curve) and reflectance (red dashed curve) of an as-grown ZnSe NW sample. (b) Plot of $(A(h\upsilon) \cdot h\upsilon)^2$, as extracted from the transmission and reflectivity curve shown in (a). The red dotted line is the linear fit of the near band-gap absorption curve. The intercept value to zero absorption gives the band-gap value (see text). The substrate is transparent in the investigated energy range (not shown).

set of data obtained for a pump fluence of 60 μJ/cm^2 is shown in Fig. 2(a) by means of a color map of ΔA versus probe energy and time delay between pump and probe pulse (in the following, simply "time delay"). ΔA is defined as the difference of the sample absorbance with and without pump excitation. Correction for the white light pulse chirp has been performed. As expected, the absorbance decreases when the probed states are occupied with photocarriers after pump excitation, and the corresponding absorbance is reduced. Notice the logarithmic scale of the time delay in Fig. 2(a) (right y axis). The spectral behavior of ΔA is shown for different time delays in Figs. 2(b) and 2(c). Figure 2(b) depicts the spectra recorded in the rise-time range, up to 600 fs, corresponding to the maximum variation, while in Fig. 2(c) we show the spectra for longer delay times, up to 880 ps. The spectra reported in Figs. 2(b) and 2(c) show two main features: a narrow dip at energies above 2.62 eV, close to the band-gap energy estimated in Fig. 1(b), and a broad band at lower energies, with a minimum in the range 2.4–2.5 eV.

The dependence of ΔA on time delay at different probe energies, corresponding to the band-gap energy or lower, is shown in Fig. 3(a) for time delays up to 20 ps. In Fig. 3(b), the detail for time delays up to 2 ps is shown for $E = 2.627$ eV,
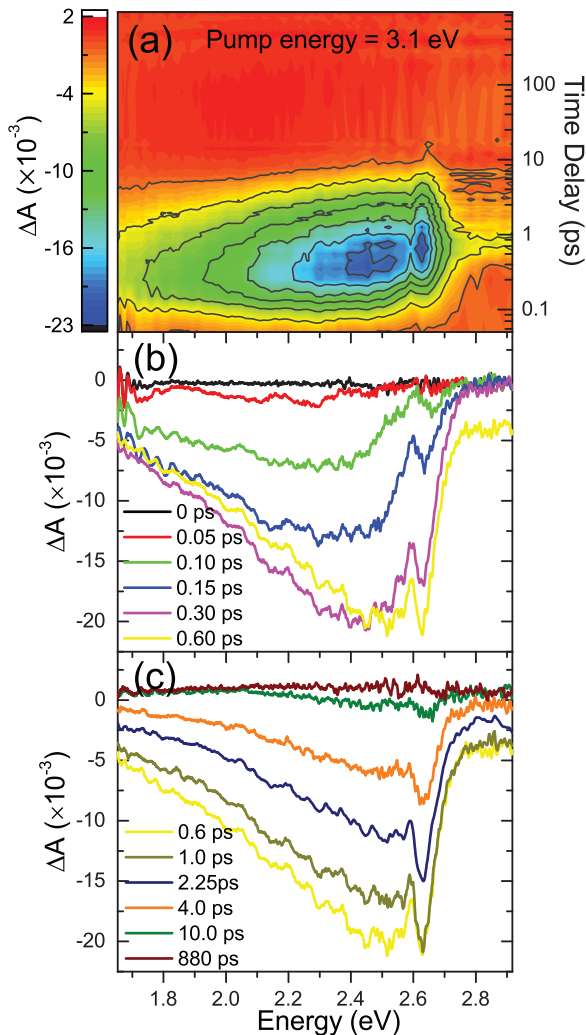
FIG. 2. (a) Two-dimensional color map of the absorbance difference ΔA as a function of probe energy (x axis) and of the delay time between pump and probe (y axis). Notice the logarithmic scale of the y axis. (b) Spectral dependence of ΔA for different delays, up to 0.6 ps. In this region, the absolute value of ΔA increases for increasing delays. (c) Same as (b) but for delay times from 0.6 to 880 ps. In this time region, the absolute value of ΔA decreases as the time delay increases. All data shown in the figure were taken at a fluence of $60\,\mu\mathrm{J/cm}^2$.

corresponding to the narrow dip minimum, in order to highlight the rising part of ΔA. As mentioned above, the maximum variation of ΔA is reached in about 600 fs, with a rise-time constant of 170 ± 60 fs. The relaxation of the signal exhibits an exponential decay with a characteristic time constant of about 4 ps. For energies below the band gap, the qualitative behavior is similar to that reported for the band-gap energy with some quantitative differences. Figure 3(c) shows the values obtained for the decay time as a function of the probe energy: a maximum is observed at energies close to the band-gap value. This behavior is independent of the excitation fluence in the range used in this paper. In general, the broad band at low energy exhibits faster dynamics than the band-gap region, both in the rising and in the decaying edges, and a smooth decrease of the decay time is observed as the probe energy decreases.

Indeed, the broad band changes lineshape as a function of time, with a clear blue-shift of its maximum, as visible in Fig. 2.

A further feature is the variation of the energy position of the narrow dip in the band-gap energy region ($E > 2.6\,\mathrm{eV}$) as a function of time (see Fig. 4). During the fast rise time, we observe a red shift of its energy followed by a slower blue shift as the ΔA signal decays. The observed red-shift energy is about 34 meV and is completely recovered after 20 ps.

Looking at long delays between pump and probe ($t \geqslant 6$ ps, depending on the probe wavelength), we observe that ΔA becomes positive by an amount that increases for increasing fluence [see Fig. 5(a)]. This is the only clear difference found in the measurements for different fluences. This positive value remains positive for the rest of the delay range under examination. As visible in Fig. 5(b), the onset on the time scale of the positive signals slightly depends on the probe energy (notice the logarithmic scale of the time axis).

Figure 6 shows the PL spectra at two different excitation intensities, varying by about one order of magnitude. At low intensities ($\sim 0.2\,\mu\mathrm{J/cm}^2$), the broad band related to defects, and the narrow NBE emission have approximately the same peak intensity. As specified later in the paper, the NBE emission is given by the contribution of excitonic and band-gap recombination. At the higher excitations ($\sim 2\,\mu\mathrm{J/cm}^2$), the defect-related band is saturated, and the NBE dominates. Figure 6(b) shows the comparison between PL and absorbance. No significant energy shift of the PL threshold is observed with respect of absorption edge in the band-gap region (also see Fig. 1).

A detail of the NBE emission is reported in Fig. 7(a) for an intermediate excitation intensity ($\sim 0.8\,\mu\mathrm{J/cm}^2$). The lineshape shows a clear shoulder on the high-energy side of the peak. Figure 7(b) shows the time-dependent PL intensity at the peak energy (2.68 eV). The PL decay time is measured to be 0.5 ns. Luminescence lineshape and decay time measured on ZnSe NWs grown with the same growth parameters on GaAs (not shown) are almost identical to those observed for the ZnSe NWs grown on glassy substrates.

IV. DISCUSSION

Both transmittance and reflectance spectra show a sharp decrease at $E > 2.6\,\mathrm{eV}$ (see Fig. 1.) It should be noted that the reflectivity spectrum substantially differs from those measured on bulk ZnSe [18,19]. The sharp decrease of the reflectivity close to the band-gap energy is a typical behavior observed in NW mats [20–22] and is due to the enhanced light absorption in the NW films, reducing the reflectivity of the overall sample. Varying wire size, morphology, and arrangement on the substrate, the optical behavior of the NW films can be gradually tuned from that of an optical coating, i.e., a thin film, characterized by a graded effective refractive index to that of an ensemble of diffuse optical reflectors [21,22]. For NW ensembles with NW size and arrangement similar to our samples, a thin film picture applies [21,22], and this justifies the use of Tauc and Menth's model to analyze transmittance and reflectance. The value of 2.63 eV for the band gap, obtained combining transmission and reflectivity data in the way described above, is smaller by about 30 meV than the values found for bulk ZnSe [18,23]. It is in good agreement,
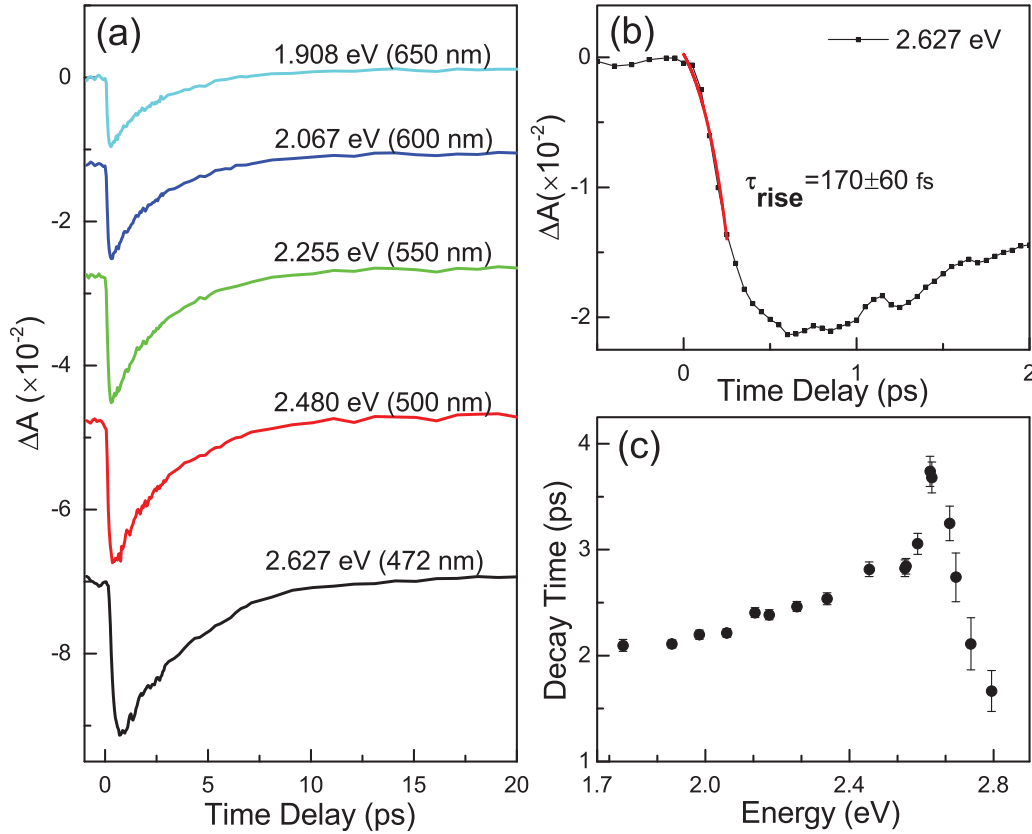
FIG. 3. (a) Time dependence of ΔA at different probe energies. (b) Detail relative to the time dependence of ΔA for $E = 2.627$ eV (energy of the narrow dip, see Fig. 2). The time scale is limited to 2 ps. (c) Spectral dependence of the decay time of ΔA.

considering that our value is given by an extrapolation in the absence of sharp features, which are, in contrast, visible in the bulk material. The absence of any indication of energy blue shifts with respect to the bulk values suggests that we do not observe any quantum confinement in our NWs.

Better agreement is obtained using as a band-gap value the energy position of the narrow ΔA dip observed in the transient absorption measurements. Its absolute intensity increases in the first 600 fs [see Fig. 3(b)]. The early rise of signal is due to
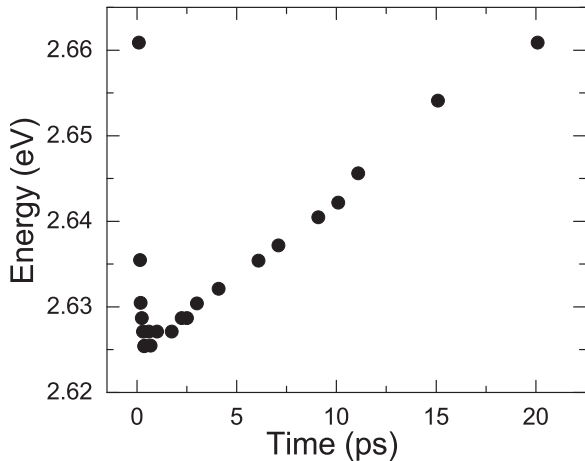
FIG. 4. Energy position of the narrow dip observed in the ΔA measurements (see Fig. 2) as a function of the pump-probe delay.

the carrier thermalization from pumped states to lower states through carrier-carrier scattering and initial longitudinal optical (LO) phonon-assisted energy relaxation [24], and it reaches maximum bleaching when the system is in a quasiequilibrium distribution of hot carriers. All probed energy states show a similar rise time. As energy state filling occurs at the probe energy, the number of free electronic states diminishes, and the corresponding absorption is reduced, a feature known as photoinduced absorption bleaching. During the rise time of the absorption bleaching, a red shift of the minimum position of the narrow dip is observed. This red shift reaches a maximum of 34 meV at about 600 fs of pump-probe delay. The red shift hence accompanies the absorption bleaching that is the carrier density increase at the band-gap energy. Consequently, we can attribute the red shift to band-gap renormalization as the result of many-body effects [25]. The highest electron-hole density is hence reached at 600 fs and is in very good agreement with time delays measured in other materials [26]. This is an important aspect, indicating that many-body effects and carrier-phonon scattering are not significantly affected by the NW shape and size.

According to a model described by Hartmann *et al.* [25], the band-gap shift is related to the free carrier density, n, and carrier temperature, T_c, by the following equation,

$$\Delta E_g(n, T_c) = -\frac{4.64 \left(na_B^3\right)^{1/2} R_{exc}}{\left[na_B^3 + \left(\frac{0.107 k_B T_c}{R_{exc}}\right)^2\right]^{1/4}}, \quad (2)$$
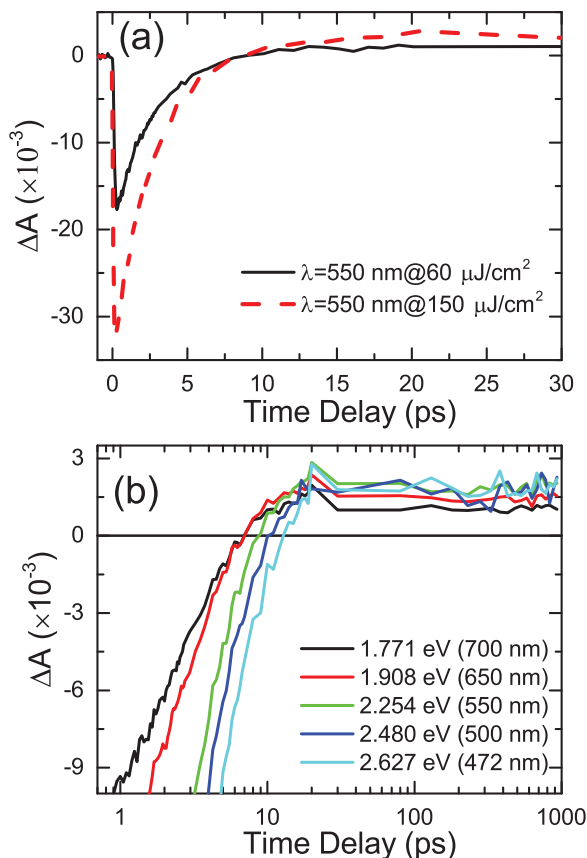
FIG. 5. (a) Time dependence of ΔA at the probe wavelength of 550 nm for two values of the pump fluence. At high fluence, a sizeable positive signal is observed at $t > 5$ ps. (b) Time dependence of ΔA for different probe energies for $150 \, \mu$J/cm^2 of pump power. Notice the logarithmic scale of the time axis.

FIG. 6. (a) The PL spectra at two different excitation intensities. (b) Comparison between absorption and luminescence spectra.

where a_B is the excitonic Bohr radius and R_{exc} is the exciton Rydberg energy. With $a_B = 3.8$ nm and $R_{exc} = 20$ meV [23], we estimate that a red shift of 34 meV is induced in ZnSe by a carrier density of about 6×10^{17} cm^{-3}, slightly above the Mott density for ZnSe, which is 4.7×10^{17} cm^{-3} as calculated by $n_M = (k_B T / 16\pi R_{exc} a_B^3)$ [27]. The value found for the highest carrier density is weakly dependent on T_c and can be considered constant if T_c does not exceed the lattice temperature (300 K) by more than 100 K.

After 600 fs, the absorption bleaching decays with a typical decay time of a few ps [see Fig. 3(c)], accompanied by a blue shift of the narrow dip (Fig. 4), an indication of a decrease of the carrier density at the band edge, with energy position that saturates for $t > 10$ ps. The saturated value of about 2.66 eV, also measured for $t \approx 0$, can be considered as a measure of the one-electron ZnSe band gap, in excellent agreement with the literature [23]. Therefore, we can state that not only state filling but also band-gap renormalization participates in the determination of the temporal behavior of the transient absorption, as also reported for bulk materials [28,29].

The presence of the broad signal, both in the transient absorption and in the PL spectra, at energies below the band gap is related to the presence of point defects in ZnSe, as also reported in ZnSe NWs grown with different methods at higher temperature [11,30]. Figures 3 and 5 show the transient absorption curves and relative decay times for selected wavelengths. We observe absorption bleaching for all wavelengths for delay times up to about 10 ps. This is different to what was observed by Othonos *et al.* [30], who report an absorption increase at short probing wavelengths in ZnSe NWs grown by vapor phase growth at 650 °C, suggesting that competitive mechanisms are present at those probe energies, namely state filling by carrier thermalization (resulting in absorption bleaching) and trapping of the carriers (resulting in photoinduced absorption). In our NWs, the single-exponential nature of the absorption bleaching decay indicates that state filling prevails for the first 5–10 ps, with larger decay times at energies closer to the band-gap energy [see Fig. 5(b)]. On the other hand, for long time delays, we ascribe the positive signal shown in Fig. 5 to photoinduced absorption by trapped carriers, as proposed for ZnSe NWs [30,31] and other materials [29,32]. Near the end of the hot carrier relaxation process (roughly 1–15 ps), an excess population of trapped carriers can be found at the defect states. As a result, there is higher probability for those carriers to be re-excited by absorbed photons. The presence of this process only at delay times larger than 5–10 ps is an indication that in our NWs defect states have negligible effects on carrier thermalization at short times because the defect density is lower than the carrier density involved in the absorption bleaching dynamics. The behavior observed here is in contrast to what is observed in ZnSe NWs grown at higher temperatures [30,31] and is an indication that low-temperature
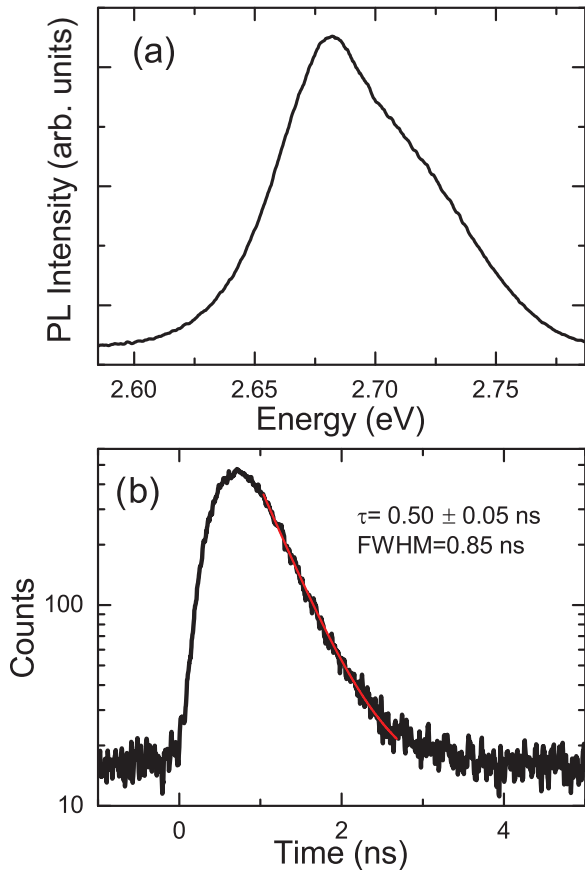
FIG. 7. (a) The NBE emission. (b) Time dependence of the PL at the peak energy (2.68 eV).

growth is a good strategy to obtain high-quality ZnSe NWs. The rising time of the defect-related band is very fast, with typical time constant ranging from 50 to 150 fs, shorter than for the band-gap signal (∼170 fs). This rise time is shorter than the decay time of the NBE signal (several ps). This feature suggests that the fast rising time of the broad band might originate from hot electron trapping where photoexcited carriers jump directly to trapped states without cooling down to the band-edge first [33].

As already mentioned, the decay time for absorption bleaching has a maximum around the band-gap energy (a value varying in time because of band-gap renormalization, see the above discussion of Fig. 4). For energies above the band gap, the shorter decay time can be understood as being due to the electrons' (holes') cooling, which is needed to reach the energetically more favorable, and hence more stable, bottom (top) of the conduction (valence) band. A slight increase of the decay time is observed at higher pump fluence (not shown) that can be explained as being given by an increased screening of the carrier-phonon interaction [34,35]. The shorter decay time observed at higher energy points towards the absence of hot-phonon effects in our measurements, in contrast to what is observed in ZnSe epilayers for similar carrier density [24]. This despite the large excess of energy of the hot carriers injected by the pump (0.47 eV, about 15 times the LO phonon energy [23]).

The decreasing decay time for decreasing probe energy below the band gap can be explained by increasing carrier-phonon interaction as the defect binding energy increases [36].

At this point we wish to comment that, diversely from other NW systems [37–39], we do not observe any contribution of the Au NP seeds to the transient absorption signal in our ZnSe NWs.

We now come to discuss the emitting characteristics of our ZnSe NWs. The PL spectra of Fig. 6 show two defect-related bands (D1 and D2), usually observed in both bulk [40,41] and NWs [11,42] ZnSe. A further typical feature for ZnSe [40,42] is that the D2 band, at lower energies, is more intense than D1 at room temperature, in contrast to what was observed at low temperature [14]. At low excitation fluence, the peak intensity of the defect-related band is about the same of the NBE emission, while by increasing the excitation intensity by one order of magnitude, the NBE is largely dominant. A closer look at the NBE emission shows that is composed of two contributions, a main one at 2.68 eV and a shoulder shifted by 20–25 meV towards higher energies [see Fig. 7(a)]. This lineshape and the energy shift [23] indicate that excitonic recombination is still observed at room temperature, as also observed in high-quality ZnSe thin films, suggesting that exciton-related nonlinear effects, observed in ZnSe thin films [43], could be also observed and exploited in ZnSe NWs. The correspondence of absorbance and PL edge energies, shown in Fig. 6(b), suggests that no extrinsic contribution is observed in the NBE region. Finally, the luminescence decay time of the NBE band is measured to be about 0.5 ns. This value is independent of the excitation intensity, as also reported in other II-VI NWs [44]. The measured decay time reflects the high quality of our NWs, especially considering that as the NW sidewalls are not protected by any shell, the decay time is probably influenced by surface-related nonradiative recombination channels. Nevertheless, the measured decay time is not very different from the value measured in nominally undoped ZnSe films (1.7 ns) and is longer than that measured in doped ZnSe films (⩽0.24 ns, depending on doping type), all grown by MBE [45]. It is also longer than in ZnTe/ZnCdTe core-shell structures [44], where a shell protects the active ZnTe core. We also point out that despite the ensemble character of our sample, the decay time is extracted by using a single decay time, a feature that gives support about the homogeneity of the NWs physical properties in our samples.

V. CONCLUSIONS

We have given a detailed and comprehensive picture of the ultrafast carrier dynamics and optical properties of ZnSe NWs grown by MBE at 300 °C. The use of a specially designed sample allowed us to perform all measurements on single samples. As expected for NW arrays, light trapping at the band-gap energy has been observed in reflectivity measurements. Fast transient absorption spectroscopy has revealed the presence of absorption bleaching and of a sizeable red shift of the NBE signal that has been explained as being due to band-gap renormalization induced by many-body effects. The band-gap renormalization has a rise-time constant of about 170 fs. The red shift starts to recover after 600 fs and decreases with a time constant of a few picoseconds.

Similar decay times are measured for the absorption bleaching, with small differences depending on the probe energy. The fast transient absorption measurements have also shown absorption bleaching at energies related to the presence of point defects in our NWs. Only after such a delay time do we observe a positive absorption variation due to defect-related photoinduced transitions. This positive absorption is sizeable only at high fluences. Finally, PL shows the presence of excitonic recombination at room temperature and the quick saturation of the defect-related emission. The characteristic decay time of the luminescence is 0.5 ns. Our data give one of the most complete pictures of transient and quasistationary optical properties of a semiconductor NW system. All of these features indicate that our ZnSe NWs behave similarly to high-quality epitaxial films, although they have been grown on amorphous substrates, opening the possible employment of ZnSe NWs for integration in low-cost microelectronics. Finally, our data confirm that similarly to what is necessary for epitaxial films, a low growth temperature results in good optical properties of ZnSe NWs.

[1] Y. Ma, X. Guo, X. Wu, L. Dai, and L. Tong, Adv. Opt. Photon. **5**, 216 (2013).

[2] C. Couteau, A. Larrue, C. Wilhelm, and C. Soci, Nanophotonics **4**, 90 (2015).

[3] H. Morkoç, S. Strite, G. B. Gao, M. E. Lin, B. Sverdlov, and M. Burns, J. Appl. Phys. **76**, 1363 (1994).

[4] M. I. B. Utama, M. de la Mata, C. Magen, J. Arbiol, and Q. Xiong, Adv. Funct. Mater. **23**, 1636 (2013).

[5] K. Imai, K. Kumazaki, T. Haga, and Y. Abe, J. Cryst. Growth **91**, 617 (1988).

[6] R. Calarco, R. J. Meijers, R. K. Debnath, T. Stoica, E. Sutter, and H. Lüth, Nano Lett. **7**, 2248 (2007).

[7] S. K. Chan, Y. Cai, I. K. Sou, and N. Wang, J. Cryst. Growth **278**, 146 (2005).

[8] Y. Cai, S. K. Chan, I. K. Sou, Y. F. Chan, D. S. Su, and N. Wang, Adv. Mater. **18**, 109 (2006).

[9] B. Xiang, H. Z. Zhang, G. H. Li, F. H. Yang, F. H. Su, R. M. Wang, J. Xu, G. W. Lu, X. C. Sun, Q. Zhao, and D. P. Yu, Appl. Phys. Lett. **82**, 3330 (2003).

[10] J. Zhuang, Y. Liang, X. D. Xiao, and S. K. Hark, J. Phys. Chem. C **116**, 8819 (2012).

[11] U. Philipose, T. Xu, S. Yang, P. Sun, H. E. Ruda, Y. Q. Wang, and K. L. Kavanagh, J. Appl. Phys. **100**, 084316 (2006).

[12] R. S. Wagner and W. C. Ellis, Appl. Phys. Lett. **4**, 89 (1964).

[13] A. Colli, S. Hofmann, A. C. Ferrari, C. Ducati, F. Martelli, S. Rubini, S. Cabrini, A. Franciosi, and J. Robertson, Appl. Phys. Lett. **86**, 153103 (2005).

[14] V. Zannier, F. Martelli, V. Grillo, J. R. Plaisier, A. Lausi, and S. Rubini, Phys. Stat. Sol. RRL **8**, 182 (2014).

[15] V. Zannier, V. Grillo, F. Martelli, J. R. Plaisier, A. Lausi, and S. Rubini, Nanoscale **6**, 8392 (2014).

[16] A. M. Fox, *Optical Properties of Solids*, Vol. 3 (Oxford University Press, New York, 2001).

[17] J. Tauc and A. Menth, J. Non-Cryst. Solids **8-10**, 569 (1972).

[18] M. Cardona, J. Appl. Phys. **32**, 2151 (1961).

[19] J. P. Walter, M. L. Cohen, Y. Petroff, and M. Balkanski, Phys. Rev. B **1**, 2661 (1970).

[20] R. A. Street, W. S. Wong, and C. Paulson, Nano Lett. **9**, 3494 (2009).

[21] A. Convertino, M. Cuscunà, and F. Martelli, Nanotechnology **21**, 355701 (2010).

[22] A. Convertino, M. Cuscunà, S. Rubini, and F. Martelli, J. Appl. Phys. **111**, 114302 (2012).

[23] O. Madelung, M. Schulz, and H. Weiss (eds.), *Semiconductors*, Landolt-Börnstein, New Series, Group III, Vol. 17b, Semiconductors (Springer Verlag, Berlin, 1987), and references therein.

[24] M. Mehendale, S. Sivananthan, W. Pötz, and W. A. Schroeder, J. Electron. Mater. **27**, 752 (1998).

[25] M. Hartmann, R. Zimmermann, and H. Stolz, Phys. Stat. Sol. (b) **146**, 357 (1988).

[26] C. V. Shank, R. L. Fork, R. F. Leheny, and J. Shah, Phys. Rev. Lett. **42**, 112 (1979).

[27] Q. Zhang, X. Liu, M. I. B. Utama, J. Zhang, M. de la Mata, J. Arbiol, Y. Lu, T. C. Sum, and Q. Xiong, Nano Lett. **12**, 6420 (2012).

[28] see, e.g., B. R. Bennett, R. A. Soref, and J. A. del Alamo, IEEE J. Quantum Electron. **26**, 113 (1990).

[29] C. S. Kim, Y. D. Jang, D. M. Shin, J. H. Kim, D. Lee, Y. H. Choi, M. S. Noh, and K. J. Yee, Opt. Express **18**, 27136 (2010).

[30] A. Othonos, E. Lioudakis, U. Philipose, and H. E. Ruda, Appl. Phys. Lett. **91**, 241113 (2007).

[31] A. Othonos, E. Lioudakis, D. Tsokkou, U. Philipose, and H. E. Ruda, J. Alloys Compd. **483**, 600 (2009).

[32] U. Siegner, R. Fluck, G. Zhang, and U. Keller, Appl. Phys. Lett. **69**, 2566 (1996).

[33] M. Cadirci, S. K. Stubbs, S. M. Fairclough, E. J. Tyrrell, A. A. R. Watt, J. M. Smith, and D. J. Binks, Phys. Chem. Chem. Phys. **14**, 13638 (2012).

[34] Q.T. Vu and H. Haug, Phys. Rev. B **62**, 7179 (2000).

[35] E. J. Yoffa, Phys. Rev. B **23**, 1909 (1981).

[36] F. A. P. Osório, M. H. Degani, and O. Hipólito, Phys. Rev. B **52**, 4662 (1995).

[37] D. Tsokkou, A. Othonos, and M. Zervos, J. Appl. Phys. **106**, 084307 (2009).

[38] A. Othonos, M. Zervos, and D. Tsokkou, Nanoscale Res. Lett., **4**, 828 (2009).

[39] We have performed ultrafast transient absorption measurements on Au seed NPs on silica NWs that show a very different behavior. First, the Au NP signal is limited to the range 500–580 nm; second, much slower decay times have been measured for the Au plasmon signal than for the ZnSe data reported here: L. di Mario, L. Tian, D. Catone, P. O'Keeffe, S. Turchini, and F. Martelli, unpublished results.

[40] S. Fujita, H. Mimoto, and T. Noguchi, J. Appl. Phys. **50**, 1079 (1979).

[41] J. A. García, A. Remon, A. Zubiaga, V. Muñoz-Sanjosé, and C. Martines-Tomás, Phys. Stat. Sol. (a) **194**, 338 (2002).

[42] G. Xing, J. Luo, H. Li, B. Wu, X. Liu, C. H. A. Huan, H. J. Fan, and T. C. Sum, Adv. Optical Mater. **1**, 319 (2013).

[43] N. Peyghambarian, S. H. Park, S. W. Koch, A. Jeffery, J. E. Potts, and H. Cheng, Appl. Phys. Lett. **52**, 182 (1988).

[44] M. Szymura, Ł. Kłopotowski, A. A. Mitioglu, P. Wojnar, G. Karczewski, T. Wojtowicz, D. K. Maude, P. Plochocka, and J. Kossut, Phys. Rev. B **93**, 155429 (2016).

[45] J. S. Massa, G. S. Buller, A. C. Walker, J. Simpson, K. A. Prior, and B.C. Cavenett, Appl. Phys. Lett. **64**, 589 (1994).